Current Trends in Technology and Science
ISSN : 2279-0535. Volume : 3, Issue : 2

3D Modeling of a Vertical Junction Polycrystalline Silicon Solar Cell Under Monochromatic Illumination in Frequency Modulation

Aminata GUEYE CAMARA, Ndeye THIAM, Idrissa GAYE, Sahin GÔKAN and Grégoire SISSOKO
Laboratory of Semiconductors and Solar Energy, Physics Department, Faculty of Science and Technology, University Cheikh Anta Diop, Dakar, Senegal (gsissoko@yahoo.com)

Abstract **- This work present a theoretical 3D study of a vertical junction polycrystalline silicon solar cell illuminated by a monochromatic light and in frequency modulation. Based on the excess minority carrier's density, the photocurrent density and the photovoltage are calculated. The solar cell dynamic impedance defined as the ratio of the photovoltage by the photocurrent, is then determined. The dynamic impedance module and phase are then studied and we exhibited the effects of grain size, grain boundary recombination velocity, junction recombination velocity and illumination wavelength.**

Keywords **- vertical junction – impedance – frequency modulation.**

I. INTRODUCTION

Given the low conversion efficiency of solar cells (M. A. Green, 1995), many researchers have been conducted to increase this conversion efficiency by improving existing structures by passivating quasi-neutral regions (T. Dullweber et al., 2011; T. Dullweber et al., 2012), adding a back surface field (L. M. Koschier et al., 1998; Kaminski et al., 2002) or by creating novel structures like vertical junction (Terheiden et al., 2000; R. Sarfaty et al 2011), triple junction (Meusel et al., 2007) and bifacial (G. Untila et al, 2008; C. Duran et al., 2010) solar cells.
In this work we will show the effects of illumination wavelength, grain size, grain boundary recombination velocity and junction recombination velocity on the dynamic impedance of a vertical parallel junction solar cell.

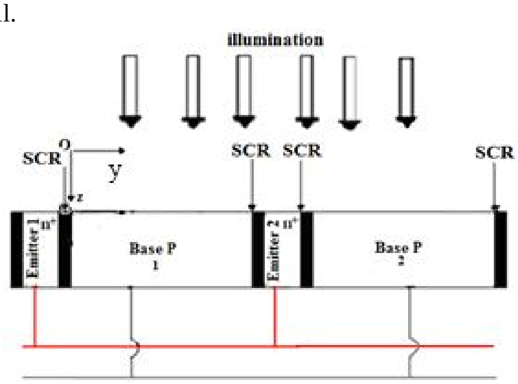

Figure 1: Vertical parallel multijunction solar cell.

II. THEORY

II.1 Model assumptions

Figure 1 illustrates the interconnection for a vertical parallel multijunction solar cell. Our 3D simulations are based on the following model for the vertical junction cell (fig2):

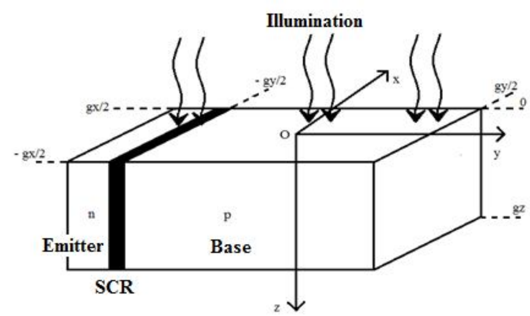

Figure 2: Solar cell's unit grain

gx and gy are the grain size, gz is the base depth along z axis.
We made the following assumptions:

- Emitter thickness and contribution are neglected (A. Dieng et al., 2011; A. Thiam et al., 2012).
- Illumination on the z=0 plane is uniform so that generation rate depend only on the depth z in the base (J. Dugas, 1994).

II.2 Excess minority carrier's density

When the solar cell is illuminated with a monochromatic light in frequency modulation, the excess minority carrier's density verifies the following equation:

$$D_n \cdot \nabla^2 \delta_n(x,y,z,t) - \frac{\delta_n(x,y,z,t)}{\tau_n} + G(z,t) = \frac{\partial \delta_n(x,y,z,t)}{\partial t}$$

D_n is the diffusion constant, t_n is the excess minority carrier's lifetime and G(z,t) is the carrier's generation rate at the depth z and time t. G(z,t) can be written as (H. J. Moller, 1993; L. Bousse et al 1994):

$$g(z) = \alpha(\lambda) \cdot (1 - R(\lambda)) \cdot I_o \cdot e^{-\alpha(\lambda) \cdot z}$$

(2)

α is the absorption coefficient for a given wavelength, R is the refractive index and Io the incident photon flux. R, α, and Io are obtained from (M. A. Green, 2008).
Replacing eq.(2) and eq.(3) into eq.(1) lead to:

ISSN : 2279-0535. Volume : 3, Issue : 2

δ is the spatial part of the excess minority carriers density .
Solution of eq. (4) is given by the following expression (Dugas, 1994):

$$\delta_n(x,y,z)=\sum_k\sum_j F_{kj}(y)\cos(C_k x)\cdot\cos(C_j z)$$

with

$$F_{kj}=A_{kj}\cdot ch(\frac{y}{L_{kj}})+B_{kj}\cdot sh(\frac{y}{L_{kj}})-\frac{\alpha(1-R)\cdot I_0}{L_{kj}^2\cdot\alpha^2-1}\cdot\frac{L_{kj}^2}{D_{kj}}\cdot e^{-\alpha\cdot z}$$

and

$$D_{kj}=\frac{Dn\cdot C_k(2C_k gx-\sin(2C_k gx))\cdot(2C_j gz-\sin(2C_j gz))}{16\cdot\frac{\alpha\cdot C_j\cdot C_k}{\alpha^2+C_j^2}(2\sin(C_k\cdot\frac{gx}{2}))\cdot(1+\frac{C_j}{\alpha}\sin(C_j\cdot\frac{gz}{2})-\cos(C_j\cdot gz)\cdot e^{-\alpha\cdot gz})}$$

Coefficients A_{kj} and B_{kj} are determined from the following boundary conditions (H. L. Diallo et al, 2008):

- At the junction (y = gy/2):

$$D_n\left.\frac{\partial\delta_n(x,y,z)}{\partial y}\right|_{y=-\frac{gy}{2}}=Sf\cdot\delta_n(x,y,z)\Big|_{y=-\frac{gy}{2}}$$

- In the middle of the base (y = 0):

$$D_n\left.\frac{\partial\delta_n(x,y,z)}{\partial y}\right|_{y=0}=0$$

- At the grain boundaries (x=gx/2; x=-gx/2):

$$D_n\left.\frac{\partial\delta_n(x,y,z)}{\partial x}\right|_{x=-\frac{gx}{2}}=Sg\cdot\delta_n(x,y,z)\Big|_{x=-\frac{gx}{2}}$$

$$D_n\left.\frac{\partial\delta_n(x,y,z)}{\partial x}\right|_{x=\frac{gx}{2}}=-\,Sg\cdot\delta_n(x,y,z)\Big|_{x=\frac{gx}{2}}$$

- At the incident light surface (z = 0):

$$D_n\left.\frac{\partial\delta_n(x,y,z)}{\partial z}\right|_{z=0}=Sav\cdot\delta_n(x,y,z)\Big|_{z=0}$$

- At the back surface (z = gz):

$$D_n\left.\frac{\partial\delta_n(x,y,z)}{\partial z}\right|_{z=gz}=-\,Sar\cdot\delta_n(x,y,z)\Big|_{z=gz}$$

Sf is the junction recombination velocity, Sgb is the grain boundary recombination velocity, Sav is the front surface recombination velocity and Sar is the back surface recombination velocity.
From the excess minority carrier's density, we can derive the photocurrent density and photovoltage.

II.3 Photocurrent density

In a 3D view, the photocurrent as to be taken as the gradient over the square section of the grain (x,z) plane; this gradient is then normalized to the cross section, giving the photocurrent density as:

$$J_{ph}=\frac{q\cdot D_n}{gx\cdot gz}\cdot\int_{\frac{-gx}{2}}^{\frac{gx}{2}}\int_0^{gz}\left.\frac{\partial\delta_n}{\partial y}\right|_{y=-\frac{gy}{2}}dxdz \qquad (13)$$

q is the elementary charge.

II.4 Photovoltage

The photovoltage is given from the Boltzmann relation as:

$$Vph=V_T\cdot\ln\left(1+\frac{Nb}{ni^2}\int_{-gx/2}^{gx/2}\int_0^{gz}\left(\delta\left(x,\frac{-gy}{2},z\right)dx\cdot dz\right)\right)$$

V_T = kT/q is the thermal voltage, ni is the intrinsic carriers density and Nb the base doping density.

II.5 Dynamic impedance

From the photocurrent density and the photovoltage, we derive the dynamic impedance as (A. Dieng et al, 2011):

$$Z=\frac{Vph}{Jph} \qquad (15)$$

III. Simulation Results And Discussion

We present here the results we obtained from simulation based on the set of equations derived in the previous section.

III.1 Dynamic Impedance module

Figure 3 shows the impedance module versus modulation frequency (logarithmic scale) for various grain sizes along x axis (gx).

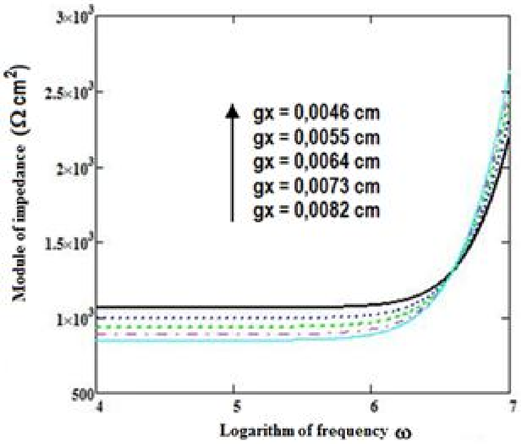

Figure 3: Impedance module versus modulation frequency (logarithmic scale) for various grain sizes gx.

One can see that for modulation frequency below about 10^6rad/s the impedance varies slightly but above this threshold, the impedance increases rapidly with modulation frequency.
Effectively, below the threshold value of modulation frequency carriers can relaxate easily so that the effect of modulation is not perceptible. Above the threshold, carriers cannot relaxate before a novel excitation occur; this lead to a diminution of carriers mobility and hence an increase of the impedance module as observed.
We also note that a decrease of grain size gx lead to an increase of the impedance module. This can be explained by the fact that carrier's mobility decreases with decreasing grain size given that lower grain size gx

Current Trends in Technology and Science
ISSN : 2279-0535. Volume : 3, Issue : 2

means more grain boundaries and then more recombination. This lead to an increase of the impedance module but this behavior is inverted above the threshold value of the modulation frequency.

We present on figure 4 the impedance module profile versus modulation frequency (logarithmic scale) for various grain sizes gz.

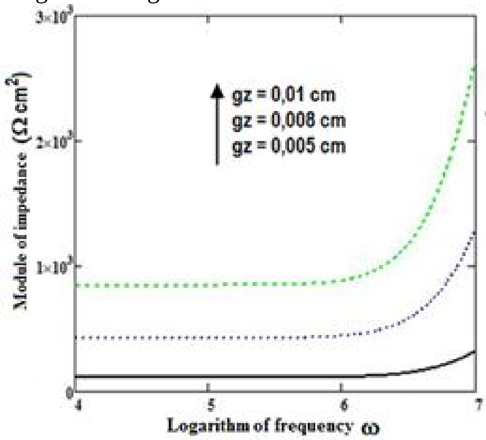

Figure 4: Impedance module versus modulation frequency (logarithmic scale) for various grain sizes gz.

This figure shows that impedance module increase with modulation frequency as noted previously; contrary to the previous case, when gz increase the impedance module also increase independently of modulation frequency. Effectively, for increasing gz, the size of the solar cell increases so that for the same operating conditions (mobility in this case) given that the size of the cell increases, the associated impedance will also increase.

Figure 5 illustrates the behavior of the impedance module for various junction recombination velocities:

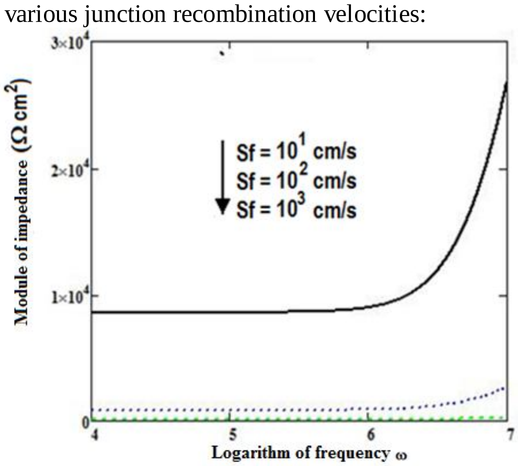

Figure 5: Impedance module versus modulation frequency (logarithmic scale) for various junction recombination velocities.

Impedance module still increase with modulation frequency and also increases with junction recombination velocity. When junction recombination increases, carrier flow through the junction increase also and then there are less and less free carriers in the base, this means a reduction of the dynamic conductivity and then an increase of the dynamic impedance.

We show on figure 6 the effects of grain boundary recombination velocity on the impedance module:

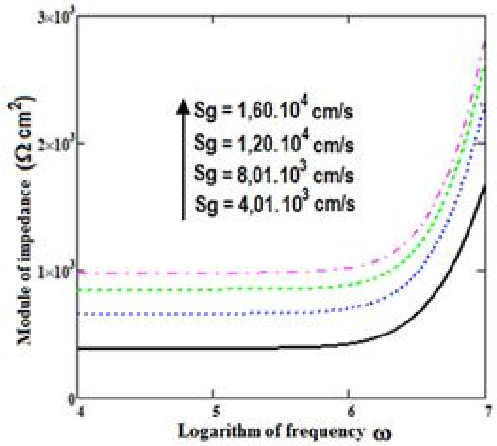

Figure 6: Impedance module versus modulation frequency (logarithmic scale) for various grain boundary recombination velocities.

This figure shows that impedance module increase with grain boundary recombination velocity; effectively, for increasing grain boundary velocity, excess minority carrier are lost faster and faster so that the free carriers concentration in the base decrease the conductivity of the decrease and the dynamic impedance increase, as observed.

III.2 Dynamic impedance phase

We present here the profile of the dynamic impedance phase (fig.7) versus modulation frequency (logarithmic scale) for various grain sizes gx.

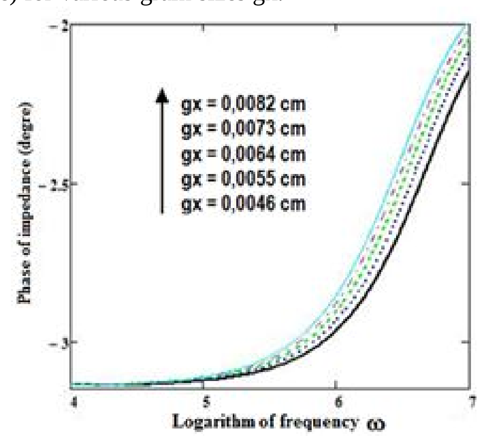

Figure 7: Impedance phase versus modulation frequency (logarithmic scale) for various grain sizes gx..

One can see that the phase shift decreases for increasing modulation frequency but the impedance phase is still negative: the vertical junction solar cell has a capacitive a capacitive behavior. This behavior is more marked for high gx values given that if gx increases the mean path between generated carriers and the junction increases so that the delay between excitation and current generation increase leading to an increase of the phase. We observe that for lower modulation frequencies (quasi-static state) the impedance phase did not vary in an appreciable manner.

Figure 8 shows the dynamic impedance phase profile versus modulation frequency for various base depth gz:

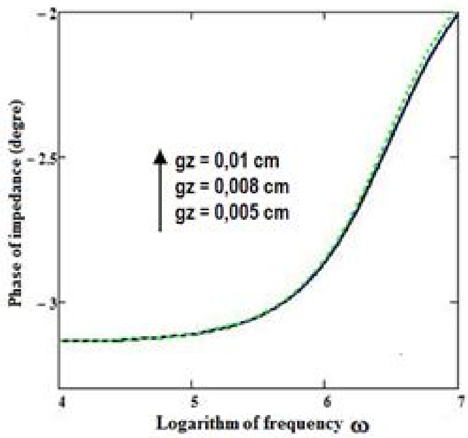

Figure 8: Impedance phase versus modulation frequency (logarithmic scale) for various grain sizes gz.

We observe that impedance phase is not very sensitive to gz.

We illustrate on figure 9 the behavior of the impedance phase for various operating points.

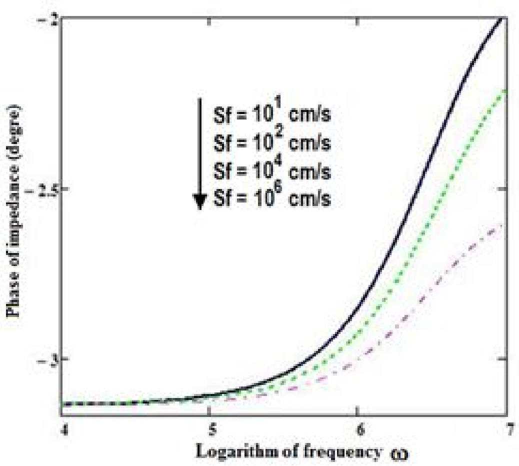

Figure 9: Impedance phase versus modulation frequency (logarithmic scale) for various junction recombination velocities.

This figure shows that impedance phase increases from short circuit to open circuit but the behavior of the vertical junction solar cell is still a capacitive as also illustrated on figure 10.

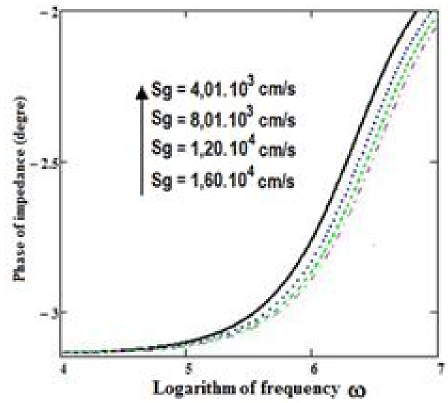

Figure 10: Impedance phase versus modulation frequency (logarithmic scale) for various grain boundary recombination velocities.

One can see that impedance phase decrease for increasing grain boundary recombination velocities; that is, the vertical junction solar cell becomes more and more capacitive as Sgb increase. This mean that recombination at grain boundaries delays the response of the vertical junction solar cell as junction recombination velocity.

IV. Conclusion

We have presented a theoretical investigation on the dynamic impedance of a vertical junction solar cell. Simulations show how the impedance module and phase are sensitive to the cell parameters (gx, gz), the modulation frequency ω and the operating point through Sf.

It seems that for all operating points the vertical junction behaves in a capacitive manner and for various grain sizes (gx, gz) and grain boundary recombination velocities, this behavior is maintained.

References

[1] Bousse, L., S. Mostarshed, D. Hafeman, M. Sartore, M. Adami et C. Nicolini, "*Investigation of carrier transport through silicon wafers by photocurrent measurements*", J. Appl. Phys. Vol.75 (8), (1994) pp 4000 – 4008

[2] Diallo, H. L., A. Seïdou Maiga, A. Wereme and G. Sissoko, *New approach of both junction and back surface recombination velocities in a 3D modelling study of a polycrystalline silicon solar cell*, The European Physical Journal Applied Physics, 42, pp 203-211, 2008.

[3] Dieng A, Zerbo I, Wade M, Maiga A S and Sissoko G 2011 Three-dimensional study of a polycrystalline silicon solar cell: the influence of the applied magnetic field on the electrical parameters, Semicond. Sci. Technol. 26095023 (9pp).

[4] Dugas, J., *3D modeling of a reverse cell made with improved multicrytalline silicon wafers*, Solar Energy Materials and solar cells 32, N°1(1994) 71-88

[5] Dullweber, T., S. Gatz, H. Hannebauer, T. Falcon, R. Hesse, J. Schmidt, and R. Brendel, *19.4% -Efficient large area rear-passivated screen-printed silicon solar cells*, Proceedings of the 26th European Photovoltaic Solar Energy Conference, Hamburg 2011, pp. 811–816.

[6] Dullweber, T., M. Siebert, B. Veith, C. Kranz, J. Schmidt, R. Brendel, B.F.P. Roos, T. Dippell, A. Schwabedissen, and S. Peters, *High-efficiency industrial-type PERC solar cells applying ICP* AlO_x *as rear passivation layer*, Proceedings of the 27th European Photovoltaic Solar Energy Conference, Frankfurt 2012, pp. 672–675.

[7] Duran, C., T. Buck, R. Kopecek, J. Libal, F. Traverso, *Bifacial solar cells with boron back surface field*, Proceedings of the 25th European Photovoltaic Solar Energy Conference and Exhibition /5th World Conference on Photovoltaic Energy Conversion, Valencia 2010, pp. 2348-2352.

[8] Green, M. A., *Self-consistent optical parameters of intrinsic silicon at 300 K including temperature coefficient*, Solar Energy Materials and Solar Cells, Volume 92, Issue 11, November 2008, pp. 1305–1310.

[9] Green, M. A., *Silicon solar cells: Advanced Principles & Practice*, Centre for Photovoltaic Devices & Systems, 1995

[10] Kaminski, A., B Vandelle, A Fave, J.P Boyeaux, Le Quan Nam, R Monna, D Sarti, A Laugier, *Aluminium BSF in silicon solar cells*, Solar Energy Materials and Solar Cells, 72 (2002), pp. 373 – 379.

[11] Koschier, L. M., Stuart R. Wenham, Mark Gross, Tom Puzzer, Alistair B. Sproul, *Low Temperature Junction and Back Surface Field Formation for Photovoltaic Devices*, Proceedings of the 2nd World Conference on Photovoltaic Solar Energy Conversion (1998), Vienna, Austria, pp.1539-1542.

[12] Sarfaty, R., A. Cherkun, R. Pozner, G. Segev, E. Zeierman, Y. Flitsanov, A. Kribus, Y. Rosenwaks, *Vertical Junction Si Micro-Cells for Concentrating Photovoltaics*, Proceedings of the 26th European Photovoltaic Solar Energy Conference, Hamburg 2011, pp. 145–147.

[13] Meusel, M., W. Bensch; T. Bergunde; R. Kern; V.Khorenko; W. Köstler; G. LaRoche; T. Torunski; W.Zimmermann; G.Strobl; W. Guter; M. Hermle; R. Hoheisel; G. Siefer; E. Welser; F. Dimroth; A.W Bett.; W. Geens; C. Baur; S. Taylor; G. Hey, *Development and production of European III-V multi-junction solar cells*, Proceedings of the 22nd European Photovoltaic Solar Energy Conference, Milano 2007, pp.16 – 21.

[14] Moller, H. J., *Semiconductors for solar cell*, Artech house, 1993

[15] Terheiden, B., G. Hahn, P. Fath, E. Bucher, *The lamella silicon solar cell*, Proceeding of the 16th European Photovoltaic Solar Energy Conference, Glasgow 2000, pp. 1377-1380.

[16] Thiam, A., M. Zoungrana, H. Ly Diallo, A Diao, N. Thiam, S. Gueye, M.M. Deme, M. Sarr and G. Sissoko, "*Influence of Incident Illumination Angle on Capacitance of a Silicon Solar Cell under Frequency Modulation*", Res. J. Appl. Sci. Eng. Technol .5(04): 1123-1128, 2012.

[17] Untila, G., T. Kost, A. Chebotareva, M. Zaks, A. Sitnikov, O. Solodukha, *Transparent Electrodes for Bifacial Silicon Solar Cells Based on Indium and Zinc Oxides*, Proceeding of the 23rd European Photovoltaic Solar Energy Conference, Valencia 2008, pp. 704 - 707.